Title

Optimization of cool roof and night ventilation in office buildings: A case study in Xiamen, China

Authors

Guo, Rui
Gao, Yafeng
Zhuang, Chaoqun
et al.

Publication Date

2020-03-01

DOI

10.1016/j.renene.2019.10.032

Peer reviewed

This document is a pre-print of the following publication:

Guo, R., Gao, Y., Zhuang, C., Heiselberg, P., Levinson, R., Zhao, X., & Shi, D. (2020). Optimization of cool roof and night ventilation in office buildings: A case study in Xiamen, China. *Renewable Energy*, *147*, 2279–2294. https://doi.org/10.1016/j.renene.2019.10.032

Optimization of cool roof and night ventilation in office buildings: a case study in Xiamen, China

Rui Guo[a], Yafeng Gao[b], Chaoqun Zhuang[b*], Per Heiselberg[a], Ronnen Levinson[c], Xia Zhao[d], Dachuan Shi[b]

[a] Department of Civil Engineering, Aalborg University, Thomas Manns Vej 23, Aalborg 9220, Denmark

[b] Joint International Research Laboratory of Green Building and Built Environment, Ministry of Education, Chongqing University, 400044, Chongqing, PR China

[c] Heat Island Group, Energy Technologies Area, Lawrence Berkeley National Laboratory, 1 Cyclotron Road, Berkeley, California 94720, USA

[d] Xiamen Academy of Building Research Group Co., Ltd., 221116, Xiamen, PR China

Abstract

Increasing roof albedo (using a "cool" roof) and night ventilation are passive cooling technologies that can reduce the cooling loads in buildings, but the research has not comprehensively explored the potential benefit of integrating these two technologies. This study combines an experiment in the summer and transition seasons with an annual simulation so as to evaluate the thermal performance, energy savings and thermal comfort improvement that could be obtained by coupling a cool roof with night ventilation. A holistic approach integrating sensitivity analysis and multi-objective optimization is developed to explore key design parameters (roof albedo, night ventilation air change rate, roof insulation level and internal thermal mass level) and optimal design options for the combined application of the cool roof and night ventilation. The proposed approach was validated and demonstrated through studies on a six-story office building in Xiamen, a cooling-dominated city in southeast China. Simulations show that combining a cool roof with night ventilation can significantly decrease annual cooling energy consumption by 27% compared to using a black roof without night ventilation and by 13% compared to using a cool roof without night ventilation. Roof albedo is the most influential parameter for both building energy performance and indoor thermal comfort. Optimal use of the cool roof and night ventilation can reduce the annual cooling energy use by 28% during occupied hours when air-conditioners are on and reduce the uncomfortable time slightly during occupied hours when air-conditioners are off.

Keywords

Cool roof; night ventilation; energy-saving; thermal comfort; sensitivity analysis; multi-objective optimization

Nomenclature

English symbols

A	Alternative
B	Attribute
C	Relative closeness to the ideal solution
E	Solar spectral irradiance
H	Hour
I	Benefit attributes
i, j	Summation index
J	Cost attributes
M	Number of alternatives
N	Number of data points
N	Number of attributes
P	Interval
Q	Simulated data
R	Measured data
$\bar{r}$	Average of the measured data
S	Matrix
$\mathcal{S}$	Solar spectrum
S	Separation of each alternative from the ideal solution
T	Temperature
Wf	Weighting factor
W	Weight of normalized value

Greek symbols

P	Albedo (solar reflectance)
Λ	Wavelength

Abbreviations

AC	Air conditioner or air conditioning
ACH	Air changes per hour
BEPS	Building energy performance simulation
COP	Coefficient of performance
CV(RMSE)	Coefficient of variation of root mean square error
HVAC	Heating, ventilation and air conditioning
LHS	Latin hypercube sampling
MBE	Mean bias error
MCA	Monte Carlo analysis
NSGA-II	Non-dominated sorting genetic algorithm II
Oh	Occupied hours in a specified period
PCM	Phase change material
POR	Percentage outside the range
TMY	Typical meteorological year
TOPSIS	Technique for order of preference by similarity to ideal solution
SRC	Standardized regression coefficient
CTF	Conduction transfer function
CHMFE	Combined heat and moisture finite element

1 Introduction

The energy consumption of buildings has increased rapidly in recent years due to several factors including the increased population, the increased demand on indoor thermal comfort and global climate changes. Approximately 40% of global energy is consumed by buildings [1], while total energy consumption by the building sector is projected to increase by 15.7% between 2013 and 2035 [2]. In China, the building sector accounts for around 25% of China's total primary energy consumption and 18% of all greenhouse gas emissions [3]. Therefore, many passive technologies have been developed to address the challenges of high building energy demands.

The total roof surface in the urban world is estimated to be around 380 billion m^2, while the roof surface accounts for over 20% of the global urban area [4]. For low or mid-rise buildings, the heat gains from roofs account for 5-10% of the annual cooling energy consumption of a building and more than 40% of the cooling energy consumption of top-floor rooms [5]. Therefore, the thermal performance of the roof is an important factor affecting the thermal comfort and the energy use of low or mid-rise buildings. Solar-reflective roofs, also known as "cool roofs", provide an effective way to reduce the energy use in buildings by reducing the solar heat gain conducted through the roof assembly [6]. The coatings in the roofs are characterized by high solar reflectance (ability to reflect sunlight, spectrum 0.3-2.5 μm) and thermal emittance (ability to emit thermal radiation, spectrum 4-80 μm) [7]. Those characteristics enable the roof to reduce solar radiation and dissipate the accumulated heat, compared with conventional building materials. Therefore, this contributes to mitigating against the increased cooling demand, reducing the energy consumption with heating penalties in conditioned buildings and improving the thermal comfort in unconditioned buildings [8]. Gao et al. [9] revealed that adopting the cool roof reduced the daily air conditioning energy use by 9% in a conditioned office building and the lower room air temperature by 1-3 °C in a naturally ventilated factory. Pisello et al. [10] also observed that cool roofs can decrease the roof bottom temperature about 10 °C and the indoor air temperature of the office area by 2-4 °C.

Night ventilation is an economical passive technique that can significantly improve thermal comfort without increasing the electricity demand [11][12]. This technology allows the outdoor cooler air to pass through the building at night so as to dissipate unwanted internal heat from buildings. Meanwhile, the building mass can be cooled during the night, which can be regarded as providing a heat sink to reduce the daytime cooling load [13]. Field and laboratory studies [14][15] illustrated that the use of night ventilation in unconditioned buildings may decrease the peak indoor air temperature of the following day up to 3 °C. For the conditioned buildings, the estimated cooling energy saving can be more than 30% [16][17], depending on the location, climatic conditions, building operation and ventilation efficiency.

Both adopting the cool roof and night ventilation may be integrated with other strategies. Chung et al. [18] evaluated the potential for reducing roof surface temperature to control urban heat island effects using the cool roof with phase change materials (PCM). Similarly, night ventilation has been applied in different climatic zones worldwide with different applications of PCMs [19][20][21]. For instance, Seong et al. [22] pointed out that the combination of PCMs with night ventilation could decrease annual cooling loads, the peak cooling load and the peak indoor air temperature by 9.3%, 11% and 0.85 °C, respectively. Some previous studies [23][24] also performed field experiments integrating night ventilation with green (vegetative) roofs for space cooling. The results show that the night ventilation can significantly mitigate the insulation effect of green roofs. AboulNaga et al. [25] investigated the optimum configuration of the wall-roof solar chimney to improve nighttime ventilation in low-rise buildings. However, the combined cooling effects of the cool roof and night ventilation have rarely been investigated. Cool roofs and night ventilation can be highly complementary and coupled techniques, particularly when they are applied to cooling-dominated areas. Increasing the roof albedo can reduce the radiative heat gain at daytime, while night ventilation can remove the indoor redundant heat during night-time.

In addition, the cooling effects of both the cool roof and night ventilation are affected by the insulation level and thermal mass level of buildings. Kolokotsa et al. [4] showed that the increased thermal mass can significantly reduce the sensible heat, while the increase of the insulation level decreased the integrated summer sensible heat and the peak indoor air temperature in European summer climates. Ran et al. [26] also presented that the energy-saving potentials of night ventilation for the building with good wall insulation are better than the building with poor wall insulation. However, previous studies focused on effects of the single input variable (e.g. envelope insulation or thermal mass) on the energy/thermal performance of the building, while the interactions among different input variables are not considered comprehensively.

This study, therefore, proposes a systematic approach to evaluate and quantify the thermal performance, cooling potential and thermal comfort improvement of combined use of the cool roof and night ventilation. A six-story office building located in a cooling-dominated city Xiamen, China is selected for both experimental and simulation studies. A global sensitivity analysis was carried out to explore the effects of roof albedo, night ventilation rate, roof insulation and internal thermal mass on the energy and thermal performance of the building. The results also offer optimal design alternatives of the aforementioned four parameters for the combined use of the cool roof and night ventilation. The organization of this paper is as follows. Section 2 introduces an overview and major steps of the thermal/energy performance evaluation and design optimization of two technologies. Section 3 presents and gives a discussion of the experimental and simulation results, including the energy-saving potential, influential design parameters and optimal design alternatives. Section 4 summarizes the conclusions are summarized.

2 Methodology

2.1 Outline of the quantitative study

A systematic approach is proposed to evaluate and quantify the combined cooling effects of the cool roof and night ventilation and to optimize the influential parameters concerned by these two technologies, as shown in Fig. 1. In the first step, the roof thermal performance and energy performance are preliminarily explored through measurements in a six-story office building. In the second step, the experimental data is used to validate the building model created for EnergyPlus [27] before simulating the annual energy-saving potential of using the cool roof and night ventilation. In the third step, a global sensitivity analysis is conducted to investigate the influences of the main design parameters on energy and thermal comfort performance of the building. In the fourth step, the multi-objective design optimization is conducted to find solutions offering superior building energy/thermal comfort performance.

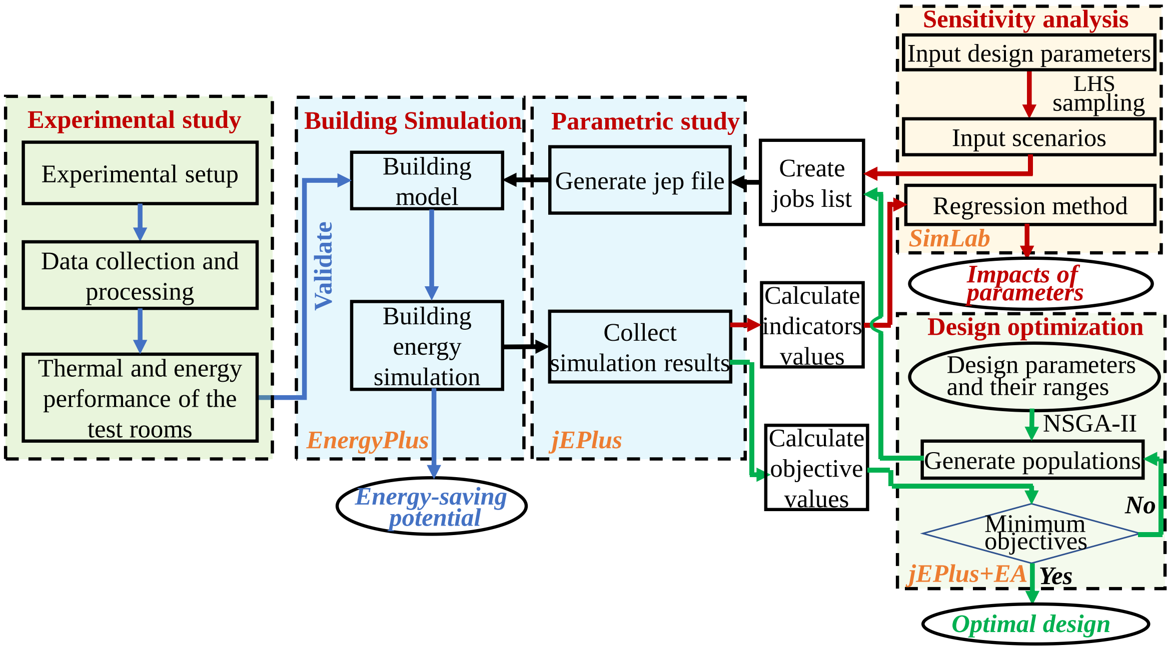

Fig. 1. Analysis flowchart for thermal/energy performance evaluation and design optimization of cool roof and night ventilation.

2.2 Experimental study

The experimental study uses a research and development centre of a company (i.e. mainly for office use), located in an industrial estate in a cooling-dominated city Xiamen. The building is actually a mid-rise building with a total of six floors. The first to four floors are used for offices while the fifth and sixth floor are used as staff dormitories and experimental rooms. The buildings in this industrial estate (i.e. in a suburb district) are generally low or mid-rise buildings (i.e. most of the buildings are not taller than six stories). Therefore, the building selected in this study can be representative of the building stock in this region. Table 1 shows the building parameters and characteristics.

Table 1 Building parameters and characteristics.

General information	
Location	Xiamen, Fujian Province, China (24.48° N 118.08° E)
Entire roof area	987.1 m^2
Orientation of long axis	North-south
Building envelope	

Window-to-wall ratio on the north wall	0.43
Wall	Three layers (insulation, brick, plasterboard) with combined thermal transmittance 0.96 W/m^2·K
Roof	Layers as depicted in Fig. 2a with combined thermal transmittance 0.86 W/m^2·K
Floor	One layer (concrete) with thermal transmittance 4.24 W/(m^2·K)
Window	Double glazing with thermal transmittance 2.91 W/(m^2·K)

Three top-floor experimental rooms with the same dimension and orientation were selected to evaluate the combined cooling effects of the cool roof and night ventilation. The roof area of each experimental room is 31.5 m^2. The roofs of two rooms were painted with reflective coatings (white and yellow respectively) and the other one was painted with a black coating for the purpose of comparison as shown in Fig. 2b. Roofs with three types of coatings were investigated to consider the effects of high, medium and low albedo roof on the building energy performance. The investigation of roofs with three coatings also ensures that there are sufficient measurements for model validation. For high-reflective coatings, the main materials include R-930 (white coating)/ PY 74 (yellow coating) titanium dioxide pigment, silicone-acrylic resin, glass beads, water and other additives. For the black coatings, the main materials include carbon black pigment, acrylic resin, water and other additives.

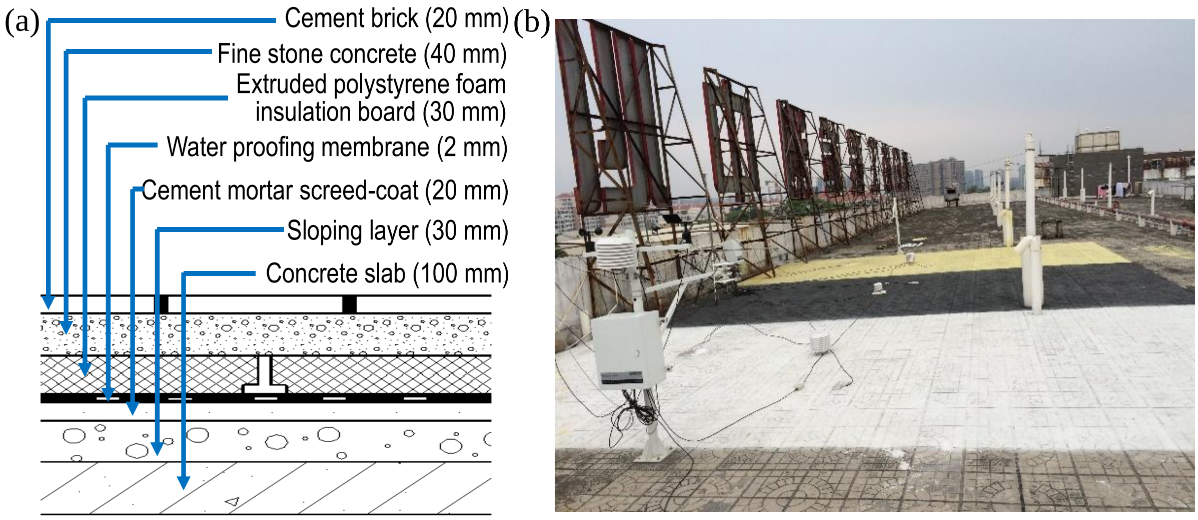

Fig. 2. (a) Cross-sectional and (b) external view of the roofs in the case-study building.

2.2.1 Properties of selected coatings

To test the optical and thermal characterization of three types of coating, the coatings were firstly sprayed on smoothly polished concrete tile samples (100 mm × 100 mm × 10 mm). Following ASTM E903-12 [28], a UV-VIS-NIR spectrophotometer (PerkinElmer Lambda 950) equipped with a 150 mm snap-in integrating sphere was used to measure the initial solar reflectance of the white, yellow and black coatings. The spectral reflectance of these three coatings (painted on specimens) was measured from 300 to 2,500 nm (shown in Fig. 3) and the albedo of each coating was then calculated according to Eq. (1).

$$\rho_s = \frac{\int_{\mathcal{S}} \rho(\lambda) E(\lambda) d\lambda}{\int_{\mathcal{S}} E(\lambda) d\lambda} \quad (1)$$

where $\rho(\lambda)$ is the spectral reflectance at wavelength λ, $\mathcal{S}$ is the solar spectrum (300 – 2,500 nm) and $E(\lambda)$ is the standard solar spectral irradiance specified in ASTM Standard G173-03 (i.e. standard air mass 1.5 direct normal and hemispherical spectral solar irradiance for 37° sun-facing tilted surface) [29].

The initial thermal emittance of coatings was measured with a portable emissometer AE1 (Model Devices & Services Co. Dallas, TX) following ASTM C1371-15 [30]. The initial albedo and thermal emittance of the white, yellow and black coatings are measured as shown in Table 2. The white coating has the highest initial albedo (0.79), followed by the yellow coating (0.57) and black coating (0.05). The measured values of the thermal emittance for white, yellow and black coatings are 0.86, 0.88 and 0.90, respectively. It is worth noting that, the thermal emittance of three coatings is very close. Virtually all construction materials except shiny and bare metals have high thermal emittance (0.80 to 0.95) [31].

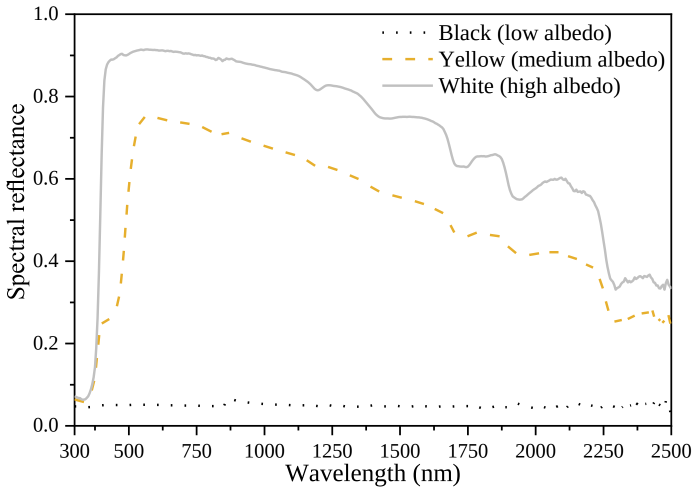

Fig. 3. Spectral reflectance of coatings over the solar spectrum (300-2,500 nm).

Table 2 Initial values of albedo and thermal emittance of three coatings.

Coating type	Albedo	Thermal emittance
White coating	0.79	0.86
Yellow coating	0.57	0.88
Black coating	0.05	0.90

2.2.2 Instrumentation, data acquisition and monitoring period

The monitored rooms were equipped with data acquisition systems which connected all sensors and recorded the measured data at a 5-min interval. The meteorological parameters (solar radiation, air temperature, air relative humidity, wind speed and rainfall) were obtained using a smart weather station. The station uses sensors placed on a 1.5 m high weather mast that is located directly on the rooftop of the building. Thermal monitoring of three rooms was performed by measuring the top and bottom surface temperature of roofs, indoor air temperature and electricity consumption of the air conditioners (ACs). Table 3 and Fig. 4 respectively present the specification of instruments and the layout of the sensors.

Table 3 Specifications of instruments.

Instrument	Make	Model	Measured parameter	Range	Accuracy
Thermal resistance	Fuyuan Feike	FY-PT100	Top and bottom surface temperature of roofs	-20 to 50 °C	± 0.2 °C
Temperature Data Logger	Inste	TH12R	Indoor air temperature	-20 to 70 °C	± 0.2 °C
Smart power meter	Letrue	LCDG-DDSD113	Electricity consumption of AC	0 to 60 A	Class 0.5
Smart weather station	Fuyuan Feike	FY-QBX	Outdoor temperature	-50 to 80 °C	± 0.2 °C
			Outdoor relative humidity	0 to 100 %	± 2%
			Wind speed	0 to 70 m/s	± 2%
			Wind direction	0 to 360°	± 3°
			Horizontal solar radiation	0 to 2000 W/m^2	± 2%

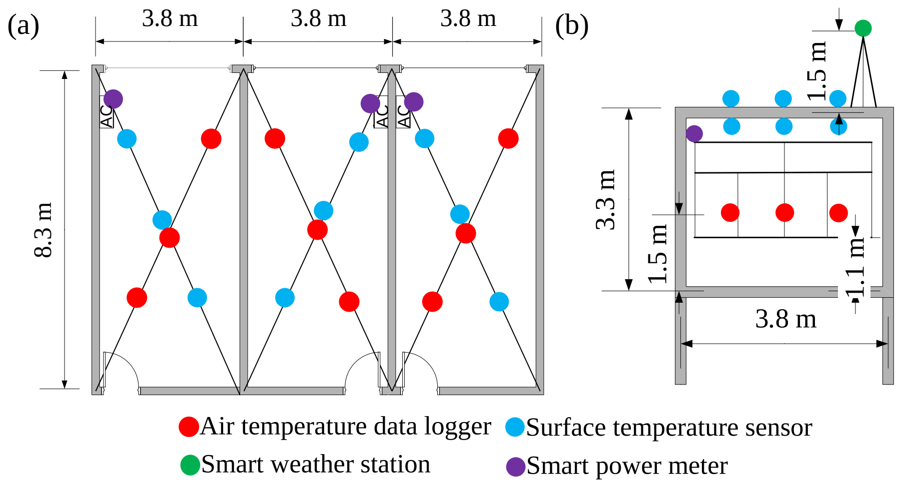

Fig. 4. (a) Vertical view and (b) side view of sensor location in the monitored rooms.

Three different scenarios were conducted to evaluate the thermal performance of cool roofs and natural ventilation in the transition season (31 March to 26 April 2015) and energy performance of cool roofs in summer (11 August to 21 August 2015). The windows were set close from 31 March to 14 April and open from 15 April to 26 April under uncontrolled conditions. The windows were closed under controlled conditions in summer. The AC operated 24 hours a day and no people worked in the office room during the test period. The AC operates 24 h/day to obtain more operational data including the AC performance data with/without the influence of solar radiation, for better validation of the building AC model. In order to reduce the influence due to the variances of occupancy, the experiment is carried out without occupancy. This is due to the fact that the occupant schedule and activity level are difficult to maintain the identical during the experiment, while the occupancy would be considered in the simulation study as further elaborated in Section 2.4.

2.3 Model validation

Before conducting the simulation analysis, a prototype building modelled for EnergyPlus was validated using the experimental data. The building model (Fig. 5a) has the same construction, layout, dimension and equipment as the case-study office building. The hourly measured meteorological data was also used as the weather input data in the simulation. To simplify the set-up procedure of the building model, the adjacent rooms (excluding the tests room) are regarded as a single thermal zone (Fig. 5b).

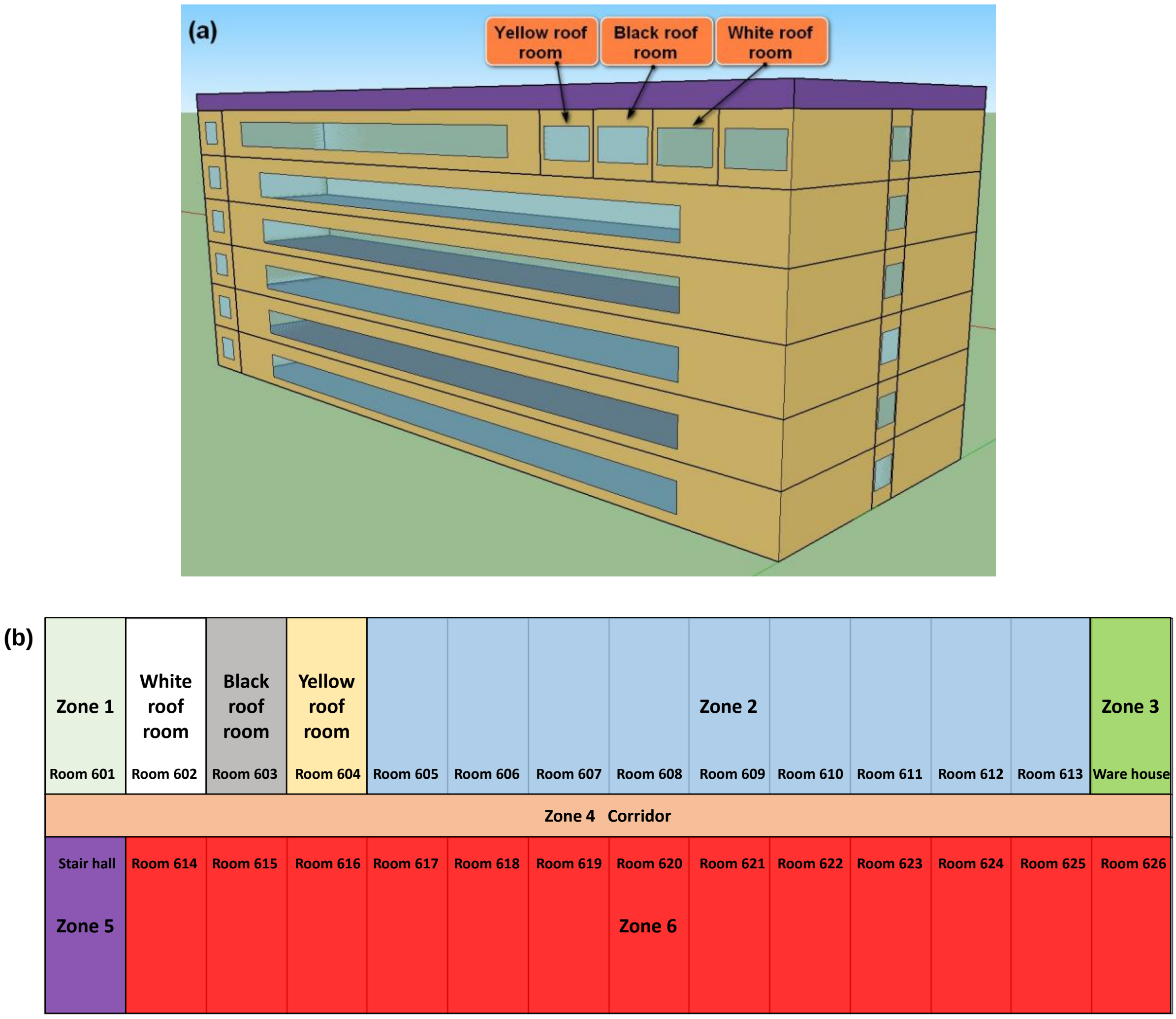

Fig. 5. (a) View of the building simulation model and (b) layout of the top floor in the building model.

As with the experimental setup, the windows of the top-floor rooms in the model were closed from 31 March to 14 April and half-open with one sliding window from 15 April to 26 April 2015. A multi-zone airflow network model in EnergyPlus was used to simulate the single-sided natural ventilation using the measured wind speed and direction data from 15 April to 26 April. The discharge coefficient of windows was set as 0.5 referring to [32] and was validated by the experimental data on the premise that other parameters of windows related to the natural ventilation were set correctly. The wind pressure coefficient was calculated automatically through the surface average calculation algorithm [33]. To validate the energy-saving benefits of using cool roofs and the performance of ACs in summer (11 August to 21 August), the AC model settings were based on the specification and operation mode of the spilt air conditioners in the tested rooms, as shown in Table 4. It is worth noting that since

Xiamen is a cooling-dominated city, only the measured cooling energy data was used for validating the AC model while the heating energy was not available for the model validation.

Table 4 Specifications of air conditioners.

Make	Model	Specifications	Unit	Value
GREE	KF-35GW/K (35356) A4C-N3	Cooling capacity	W	3,520
		Rated cooling power	W	1,105
		Maximum input power	W	1,550
		Circulating air	m^3/h	630
		Coefficient of performance (COP)	W/W	3.2
		Cooling set point	℃	26

The thermal performance of the building/room model was validated by comparing the simulated and measured top and bottom surface temperature of roofs and indoor air temperature in the transition season (i.e. from 31 March to 26 April). Meanwhile, the energy performance of the air-conditioners inside rooms was validated by comparing the simulated and measured AC electricity consumptions during the test period in summer (i.e. from 11 August to 21 August). Several acceptance criteria are commonly used for calibrating building energy performance simulation (BEPS) models [34]. The mean bias error (MBE) and coefficient of variation of root mean square error CV(RMSE) were computed using Eqs. (2) and (3) respectively.

$$\text{MBE}\ (\%) = \frac{\sum_{i=1}^{N_p}(r_i - q_i)}{\sum_{i=1}^{N_p}(r_i)} \quad (2)$$

$$\text{CV(RMSE)}\ (\%) = \frac{\sqrt{\sum_{i=1}^{N_p}(r_i - q_i)^2 / N_P}}{\bar{r}} \quad (3)$$

where r_i and q_i are the measured and simulated data points for each model instance 'i' respectively, N_p is the number of data points at interval 'p'. $\bar{r}$ is the average of the measured data points. In this study, the performance of the present building model was assessed using the hourly criteria in ASHRAE Guideline 14, as shown in Table 5 [35].

Table 5 Acceptance criteria for calibration of BEPS models.

Standard/guideline	Monthly criteria (%)		Hourly criteria (%)	
	MBE	CV (RMSE)	MBE	CV (RMSE)

ASHRAE Guideline 14	5	15	10	30

2.4 Simulation analysis

2.4.1 Annual energy simulation analysis

Xiamen is a cooling-dominated city where the cooling-only air-conditioners (i.e. no heating function) are commonly adopted and there is usually no heating system available in winter. Therefore, the annual energy consumption analysis only includes the AC cooling energy consumption in this study. To investigate the annual energy-saving potentials of cool roofs combined with night ventilation, the settings of the validated building model (in Section 2.3) were updated as followings. i). The entire roof of the model was set with a uniform albedo to eliminate the heat transfer between roofs with different albedos in the previous model. ii). The roof albedo was set to 0.6 or 0.1, representing an aged cool roof and an aged black roof, respectively [36]. iii). Typical meteorological year (TMY) data [37] of Xiamen was used as weather input.

A typical office (room 603) was used as the simulation object. It was set to be occupied by four people with a clothing thermal resistance of 0.5 clo in summer according to EN 15251 [38]. The hourly operational schedules for people, lights and electric equipment were set as 1.0 during the occupied period (08:00-18:00) and 0 for the remaining period. Internal partitions between the concerned room and adjacent zones were set adiabatic, assuming all adjacent zones have similar working conditions. Typical internal heat gains were added to the concerned rooms [39], as shown in Table 6.

Table 6 Internal heat gains per unit floor area in room 603.

Internal heat gains	Unit	Value
Person (4 people)	W/person	75
Lights	W/m^2	7
Electric equipment	W/m^2	9
Total	W/m^2	25.5

The AC operated during working hours (08:00–18:00) on weekdays when the indoor air temperature exceeded 26 ℃, while the night venting schedule was 18:00-08:00 (+1) on weekdays. It is worth noting that the night venting was only available during the hot days when the AC was required to operate on the following day. The outdoor air flowrate during occupied hours was set to 30 $m^3/(h \cdot person)$ [40]. Night mechanical ventilation and night natural ventilation were selected for comparison. The model settings of the natural ventilation system and the ACs were the same as the previously validated model, while the night mechanical ventilation was set as a balanced system with a supply fan and an exhaust fan. The specific fan power of night mechanical ventilation system fulfills the recommended “good-practice” from the technical note AIVC 65 [41]. The lower limit of indoor air temperature for night mechanical ventilation was set as 18 ℃ to avoid overcooling [42], while the temperature difference between indoor and outdoor air for night ventilation activation was set as 3 ℃ to achieve effective convection [43]. Since the maximum air change rate per hour (ACH) for night ventilation should not exceed 10 h^{-1} [44], the design ACH for night mechanical ventilation was set to 5 h^{-1} and 10 h^{-1}, respectively. It is worth noticing that the performance difference among various strategies, ranging from simple fixed-rules to complicated predictive algorithms, is small [45,46]. Therefore, a common-used night ventilation control strategy was adopted in this study. Table 7 summarizes the detailed setup information of night mechanical.

Table 7 Detailed setup information of night mechanical ventilation systems.

Night mechanical ventilation system	
System configuration	Supply fan and exhaust fan
Total design pressure rise	600 *Pa* (Both for supply fan and exhaust fan)
Fan total efficiency	0.9
Design ACH	5 h^{-1} or 10 h^{-1}
Minimum indoor air temperature	18 ℃
Activation requirements	Indoor air temperature – outdoor air temperature > 3 ℃

2.4.2 Sensitivity analysis

A sensitivity analysis was carried out to explore the key influential factors on energy/ thermal comfort performance of top-floor rooms. The global sensitivity method was selected to investigate the influence of a single input variable on the outputs when other input variables also vary simultaneously, which can explain how much variations of the outputs are accounted by the input variables. Monte Carlo analysis (MCA) and Latin Hypercube Sampling (LHS) were selected as the variance-based method and sampling method for the global sensitivity analysis [47].

Fig. 1 shows the process of conducting sensitivity analysis (upper right corner) and it is explained as follows. In the first step, SimLab [48] generates the input scenarios based on the defined range of main concerned parameters by LHS sampling method. The sample size based on LHS is 150, as the minimum number of model executions should be at least 10 times the number of variables. In the second step, jEPlus generates building simulation model descriptions (jep file) based on the job list created using the input scenarios from SimLab to run the EnergyPlus. Then jEPlus collects all the simulation results from EnergyPlus and calculates the indicator values for each scenario [49]. Finally, SimLab can conduct sensitivity measures based on the selected sensitivity analysis method. Standardized Regression Coefficient (SRC) based on the regression method is used as the global sensitivity analysis indicator by assuming the input variables are independent. The sign of SRC indicates whether the output increases (positive value) or decreases (negative value) as the related input variable increases. The larger the absolute value of SRC, the more influential the input variable [50].

Four key parameters, including roof albedo, night ventilation air flow rate, roof insulation level and internal thermal mass level, are considered in the sensitivity analysis, in order to explore their impacts on the energy and thermal performance of buildings. Table 8 shows the input parameters and their distributions. Both the parameters are independent and with uniform distribution. The roof insulation level varies as the thickness of the insulation board changes, while the surface area of internal mass made by the cast concrete determines the internal thermal mass level. It is worth noting that the coating thickness was not considered an influential factor for the following reasons: i). Yarbrough and Anderson [51] illustrated that optimum albedo of the coatings can be obtained when the thickness greater than a minimum critical thickness. The thickness of the coatings is sufficient enough to ensure the roofs with an optimum albedo in this study. ii). Roof insulation level is also a design parameter considered in this study, which covers the influences of the coating insulation due to the change of coating thickness. Table 9 shows detailed information for performance indicators.

Table 8 Input parameters range for the sensitivity analysis.

Concerned parameters		Unit	Probability distribution
P1	Roof albedo	-	**U**[a] [0.1-0.9]
P2	Night ventilation ACH	h^{-1}	**U**[a] [0-10]
P3	Roof insulation level	mm	**U**[a] [10-50]
P4	Internal thermal mass level	m^2	**U**[a] [10-80]

[a] Represents uniform distribution.

Table 9 Outputs of the sensitivity analysis.

Performance indicators		Unit	Remark
O1	Annual cooling energy use	kWh/m^2	During working hours (08:00–18:00) in the design summer year, with setpoint 26 ℃
O2	Percentage outside range (POR)	%	During working hours (08:00–18:00) in non-AC operation condition

Percentage outside range (POR) was selected as a thermal comfort indicator as shown in Eq. (4). This indicator accumulates the percentage of occupied hours in the non-AC operation time when the simulated thermal comfort level exceeds the specified comfort range in corresponding standards [52].

$$\mathrm{POR} = \frac{\sum_{i=1}^{Oh}(wf_i \cdot h_i)}{\sum_{i=1}^{Oh}(h_i)} \tag{4}$$

Here wf_i is a weighting factor depending on the comfort range. h_i represents the occupied hours and Oh is the occupied hours in a specified period. If the thermal comfort parameter exceeds the corresponding comfort range, the wf_i would be 1, otherwise it would be 0. The 80% acceptability status of ASHRAE 55 adaptive thermal comfort model applied to calculate the values of POR [53]. Larger POR indicates the indoor thermal environment is far from satisfactory.

2.4.3 Design optimization

To investigate the optimal design parameters to improve the building energy/thermal comfort performance, a multi-objective design optimization was conducted by using jEPlus+EA software [54]. One of the common-used evolutionary algorithm Non-dominated Sorting Genetic Algorithm II (NSGA-II) that adopts non-dominated sorting techniques to offer the closest solutions to Pareto-optimal solution was selected for multi-objective optimization [55] in this study. The design variables include roof albedo, night ventilation ACH, roof insulation level and internal thermal mass level. It is worth noting that, in the real applications, the ACH of night natural ventilation is determined/influenced by several factors including space orientation, wind speed and direction, ventilation control system, window open factor and discharge coefficient. Due to the dynamic characteristics of some parameters, it is difficult to quantify the ventilation effectiveness precisely. The focus of this study is to evaluate the effects of night ventilation ACH on the indoor thermal comfort/AC energy consumption; therefore, the ACH of night natural ventilation was set directly for simplicity. Annual cooling energy use and POR during occupied hours without AC operation are the two objectives to optimize (Table 9).

The process of conducting design optimization shown in the lower right corner of Fig. 1 can be explained as follows. In the first step, the NSGA-II optimizer generates the populations (sets of design parameter values) within the predefined searching ranges of the design parameters and a job list is created based on the generated design parameters. The ranges of design variables are set the same as the parameters in Table 8. In the second step, jEPlus generates building simulation model descriptions for EnergyPlus (jep files) based on the job list. jEPlus then collects all the simulation results from EnergyPlus and calculates the objective values for each scenario. Finally, the NSGA-II optimizer in jEPlus+EA further calculates the objective values until the optimization reaches convergence tolerance. For the optimization setting, the population size, maximum generation number, crossover number, mutation number and tournament selector size are set as 10, 200, 1.0, 0.2 and 2 respectively by compromising the computational cost and the accuracy of the Pareto front solutions.

The optimum solution for the multi-objective design optimization is selected by employing Technique for Order of Preference by Similarity to Ideal Solution (TOPSIS) decision-making method. The TOPSIS is based on the concept that the chosen alternatives should have the shortest geometric distance from the positive ideal solution and the longest geometric distance from the negative ideal solution [56]. The TOPSIS technique is detailed in Appendix A.

3 Results and discussion

3.1 Experimental results and model validation

3.1.1 Weather conditions

31 March to 26 April and 11 August to 21 August 2015 were selected as representative days in the transition season and summer, respectively. Most selected days are sunny days and Fig. 6 shows the solar irradiance, outdoor air temperature and relative humidity. From 31 March to 14 April, under window-closed conditions, the daily mean outdoor air temperature oscillated between 14.7 °C and 29.0 °C and the daily maximum value of global horizontal solar irradiance varied between 221 W/m^2 and 1,231 W/m^2. From 15 April to 26 April, under window-open conditions, the daily mean outdoor air temperature oscillated between 19.8 °C and 26.9 °C and the daily maximum value of global horizontal solar radiation varied between 176 W/m^2 and 1,243 W/m^2. From 11 August to 21 August, under controlled conditions (i.e.

air-conditioners are on), the daily mean outdoor air temperature oscillated between 27.5 °C and 32.3 °C and the daily maximum value of global horizontal solar radiation varied between 402 W/m^2 and 1,370 W/m^2. Due to the humid climate characteristic in Xiamen, the relative humidity is high, with average values of 72% in the transition season and 84% in summer, receptively. The statistical analysis of the wind direction and wind speed from 15 April to 26 April is presented by the wind rose diagram as shown in Fig. 7. Each concentric circle represents a different fraction of time that the wind blows from this particular direction, starting from zero at the center and increasing towards the outer circles. Most of the prevalent wind directions at the site are the east and west. All the measured weather data is, therefore, used as the inputs when the building simulation is conducted.

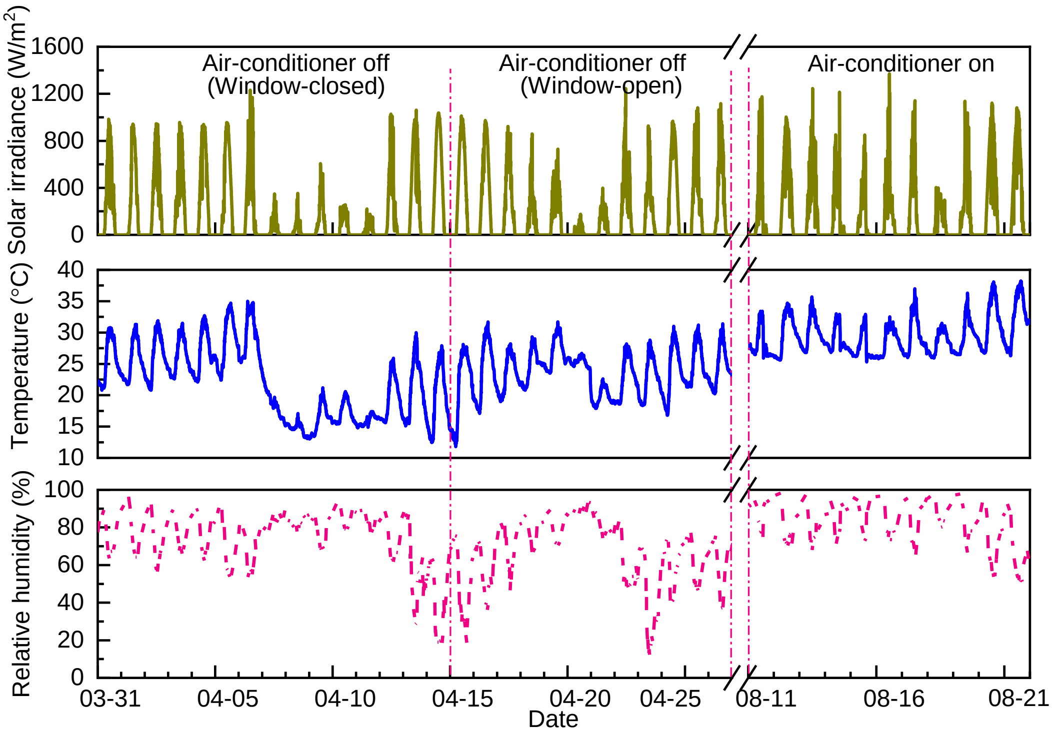

Fig. 6. Global horizontal solar irradiance, outdoor air temperature and relative humidity measured by smart weather station (sensors at 1.5 m height from the rooftop).

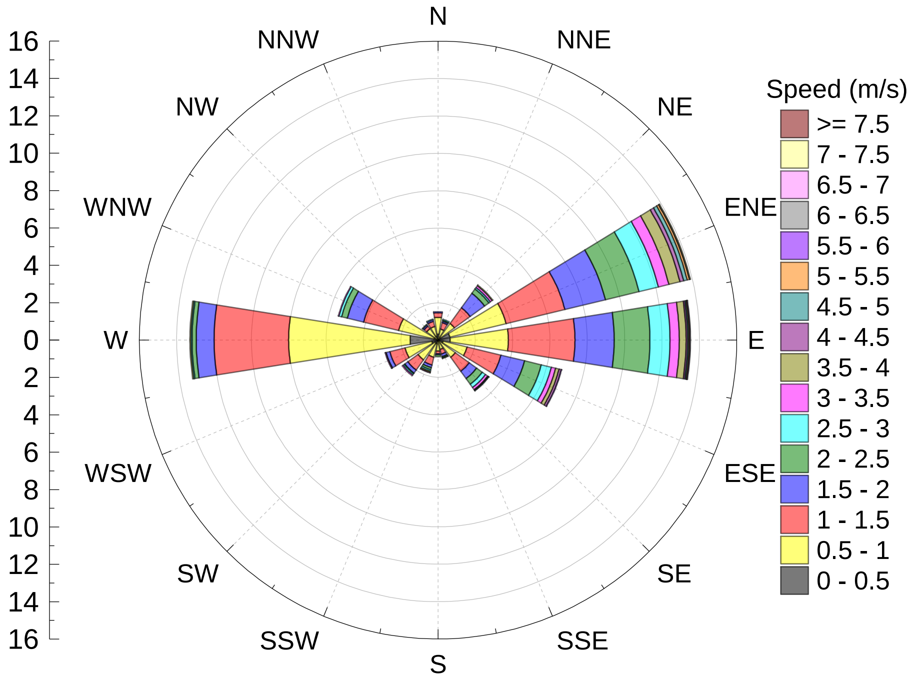

Fig. 7. The wind rose diagram from 15 April to 26 April 2015 in the experimental site.

3.1.2 Thermal performance in the transition season

Fig. 8 shows the measured data of exterior roof surface temperature, interior roof surface temperature and the indoor air temperature of the monitored rooms in the transition season (31 March to 26 April). During this period, the top of black roof peaked at 68.6 °C, while the tops of the white roof and yellow roof were up to 27.2 °C and 20.3 °C cooler, with peak temperatures of 41.4 °C and 48.3 °C, respectively. The bottom (room-facing surfaces) of the white roof and yellow roof were up to 3.1°C and 2.8°C cooler than the bottom of the black roof, respectively.

The introduction of natural ventilation influences the indoor thermal environment as shown in panels c and g of Fig. 8. The indoor air temperatures measured in white roof room and yellow roof room were 1.2 °C and 0.9°C lower than that observed in black roof room when windows were closed (31 March to 14 April). When the windows were open (15 April to 26 April), the maximum indoor air temperature decrease in both these rooms (white roof room and yellow roof room) are both around 1.3 °C lower than that observed in the black roof. In addition, the mean indoor air temperatures of white roof and yellow roof rooms are both around 25 °C, which are 0.6°C lower than that of the black roof room. This indicates the unwanted internal heat gains (i.e. the difference of heat gains between the white roof room and yellow roof room) of the yellow roof room can be removed through natural ventilation. The natural ventilation contributes to the dissipation of unwanted internal heat from the buildings.

Fig. 8 shows the measured and simulated data, including the exterior roof surface temperature, interior roof surface temperature and indoor air temperature. The mean bias error (MBE) (%) and coefficient of variation of root mean square error CV(RMSE) (%) between the measured and simulated data are calculated as shown in Table 10. The MBEs and CV(RMSE)s between the measured and simulated temperature vary between -1.8% and 3.1% and between 2.5% and 9.2%, respectively. When the uncertainties (i.e. ±0.2 ℃) of temperature sensors in Table 3 is taken into consideration, the MBEs and CV(RMSE)s between the measured and simulated temperature also fulfill the acceptance criteria of model calibration shown in Table 5. This indicates the present building model is well-established and can be used to precisely simulate the thermal performance of rooms. The discrepancies between simulated and measured data could attribute to the following reasons: 1) The meteorological data (e.g. the solar irradiance) was set as a one-hour interval, which cannot fully represent the actual weather conditions and 2) The long-wave radiation and shadings from surrounding buildings were neglected.

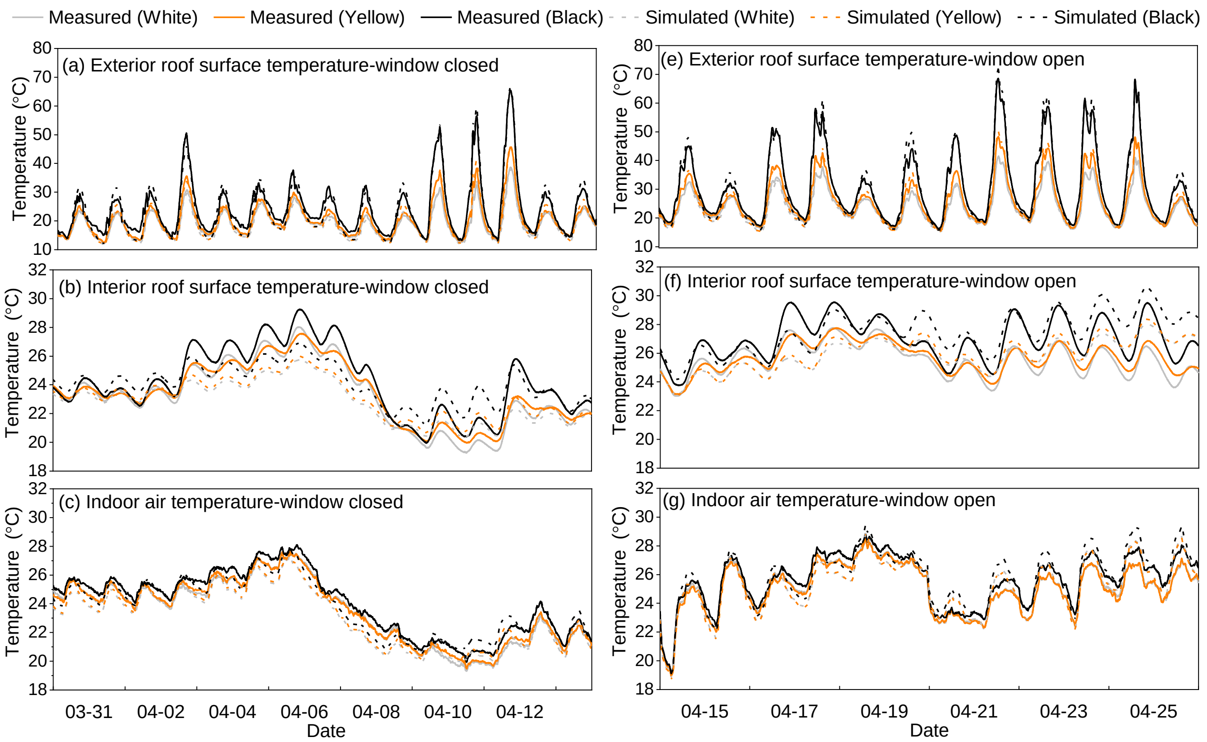

Fig. 8. Measured and simulated thermal performance in the monitored rooms.

Table 10 Model validation of thermal performance in the transition season by MBE (mean bias error) and CV(RMSE) (coefficient of variation of root mean square error).

Performance indices (%)	Window status	Exterior surface temperature			Interior surface temperature			Room temperature		
		White	Yellow	Black	White	Yellow	Black	White	Yellow	Black
MBE	Closed	3.1	2.3	2.3	2.1	1.4	0.6	1.7	1.4	1.1
CV (RMSE)		4.6	6.1	9.2	4.5	3.8	5.0	3.0	2.6	2.7
MBE	Open	1.7	0.8	-0.8	-1.2	-1.2	-1.8	-0.6	-0.6	-0.8
CV (RMSE)		3.3	4.6	6.0	4.6	3.9	4.4	2.7	2.5	2.5

3.1.3 Energy performance in summer

Fig. 9 shows the measured hourly electricity consumption of air conditioners in three rooms from 11 Aug to 21 Aug. Normalized by room roof area, the air conditioner in white roof room and yellow roof room consumed about 99 $Wh/m^2 \cdot day$ and 82 $Wh/m^2 \cdot day$ less electricity than that in black roof room, for a daily savings of about 30% and 25%, respectively.

Fig. 9 also shows the measured and simulated AC electricity consumption. Table 11 summarizes the mean bias error (MBE) (%) and root mean square error (RMSE) (%) between the measured and simulated electricity consumption of air-conditioners. It can be seen that the MBEs and CVRMSEs between the measured and simulated temperature vary between -7.6% and -4.7% and between 27.9% and 29.0%, respectively. The precision of the BEPS model is within the acceptable ranges as shown in Table 5. Therefore, the building model with the configured air-conditioning system can be used to further assess the energy-saving potentials of the cool roof and night ventilation. The discrepancies between simulated and measured data of AC electricity consumption attributes to the reason that the AC operates intermittently in the real-time environment that may consume additional energy consumption.

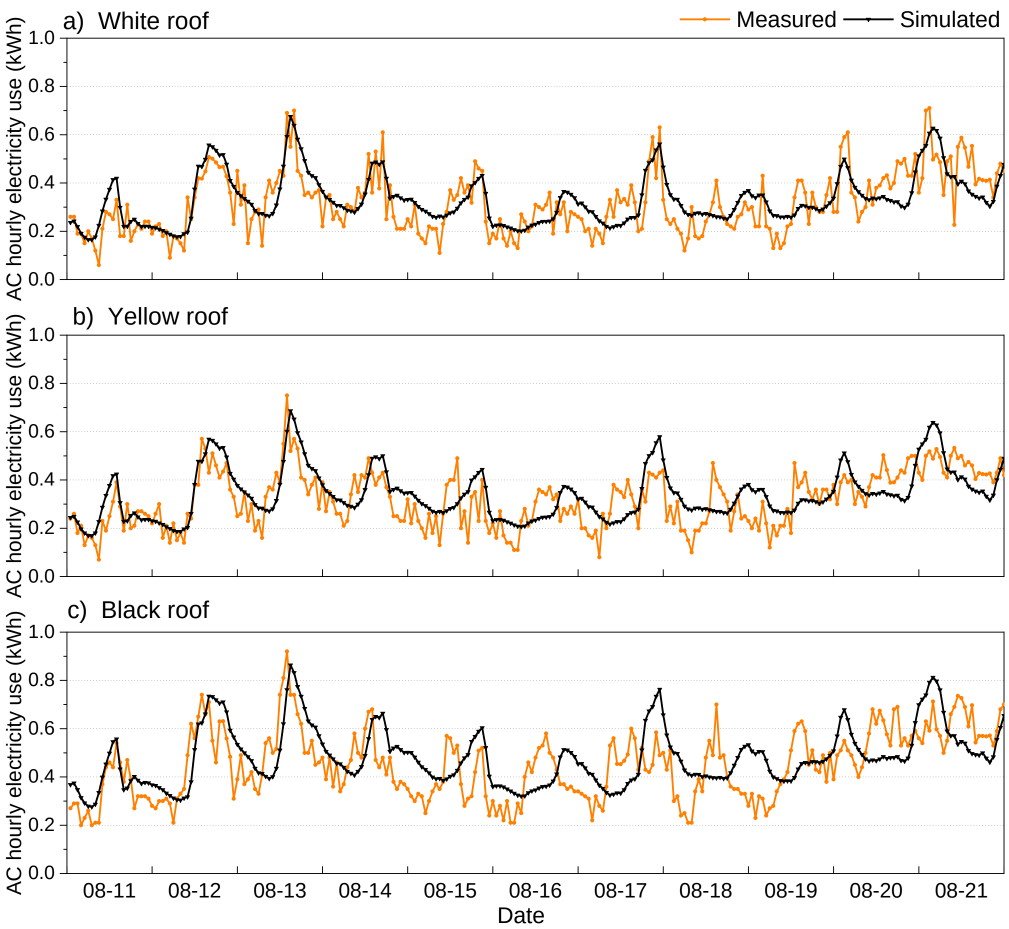

Fig. 9. Measured and simulated hourly AC electricity consumption a) white roof, b) yellow roof and c) black roof.

Table 11 Model validation of AC hourly electricity consumption in summer.

	White roof room	Yellow roof room	Black roof room
MBE (%)	-4.7	-7.6	-7.0
CVRMSE (%)	27.9	28.9	29.0

3.2 Simulated annual energy-saving potential

The energy performances of adopting different roof albedos and night ventilation modes in Typical Meteorological Year (TMY) are simulated and compared as shown in Fig. 10. The case of using the black roof only (i.e. the albedo of 0.1) is set as a base case for the purpose of comparison.

Compared with using black roof only (base case), applying the cool roof (i.e. the albedo of 0.6, case 4) on buildings can significantly reduce the annual AC electricity consumption by 6.2 kWh/m^2 (16%). The combined use of cool roofs and night mechanical/natural ventilation on buildings contributes to less AC electricity consumption as the night ventilation can remove the excess heat stored at daytime. However, when taking the fan energy use at night into account, the total cooling energy savings (i.e. considering both AC and fan electricity use) of case 5 and case 6 are only 1.5 kWh/m^2 (4%) and 4.0 kWh/m^2 (10%) respectively compared to the base case. It is worth noting that the overall cooling energy consumption adopting night mechanical ventilation and cool roof can be even higher than that of case 4 (i.e. only using the cool roof). Also, the total cooling energy use increases when the ACH of night mechanical ventilation increases. The reason is that the annual mean outdoor air temperature at night in Xiamen is relatively high, resulting in low night cooling energy-saving potential.

It can also be seen that adopting the night natural ventilation can reduce AC energy consumption and the AC energy savings are close to that of adopting the 10-ACH night mechanical ventilation. Combining the cool roof with night natural ventilation (case 7) can save 10.5 kWh/m^2 (27%) compared with that of the base case and 4.3 kWh/m^2 (13%) compared with case 4 equipped with the cool roof. It indicates that night natural ventilation contributes to more energy savings.

Integrating the black roof with night mechanical ventilation (case 1 or case 2) also consumes more total cooling energy, compared to the base case. Although the black roof combined with night natural cooling (case 3) can save cooling energy compared with the base case, its energy consumption is still 1.2 kWh/m^2 higher than that of using the cool roof only (case 4).

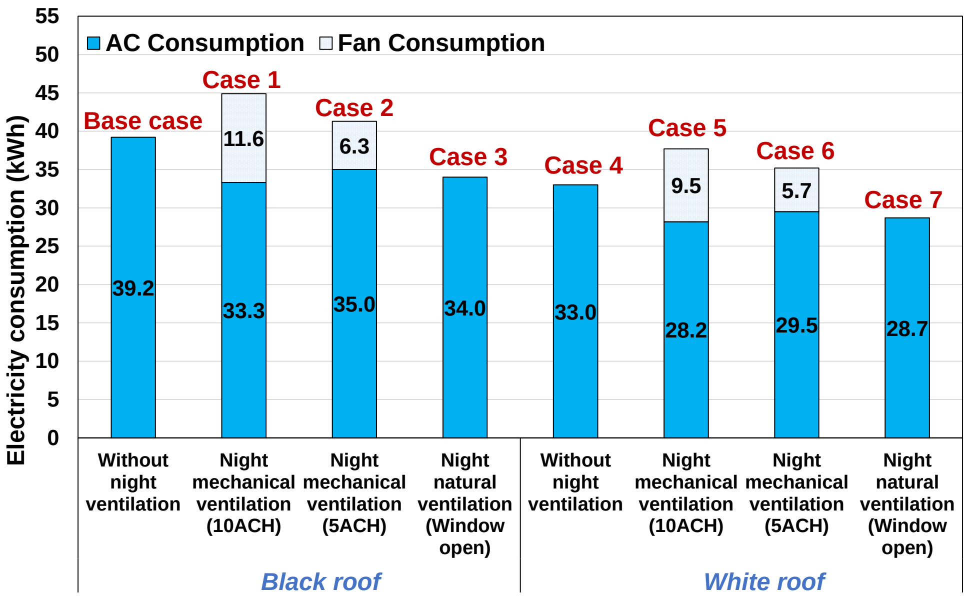

Fig. 10. The comparison of electricity consumption using different strategies.

The indoor air temperatures adopting different strategies in a typical summer night (1 June to 2 June) are compared (Fig. 11) to explain the differences of energy-saving potentials among different strategies. On the selected day, the average wind velocity was 4.9 m/s and the prevailing wind was from the south-east direction. It can be seen that after turning off the AC at 18:00 on June 1, the indoor air temperatures of all scenarios rose fast. After 20:00, the indoor air temperatures of using the cool roof only and using black roof only vary slightly, remaining about 26.5 ℃ and 30.7 ℃ respectively. The cool roof room has lower indoor air temperature at night compared with that of black roof room. One possible reason is that the excess heat stored in the building elements at daytime was released to the indoor environment and black roof room had more accumulated heat. However, when using the night ventilation, the indoor air temperatures were lower and the trend followed the profiles of outdoor air temperature. For both the cool roof and black roof rooms, using 10-ACH night mechanical ventilation yielded the lowest indoor air temperature at night, followed by using night natural ventilation and 5-ACH night mechanical ventilation. This indicates that adopting 10-ACH night mechanical ventilation can reduce the AC energy use at daytime. The combined use of the cool roof and 10-ACH night mechanical ventilation has the lowest indoor air temperature among all scenarios, with an average temperature of 26.5 ℃ at night.

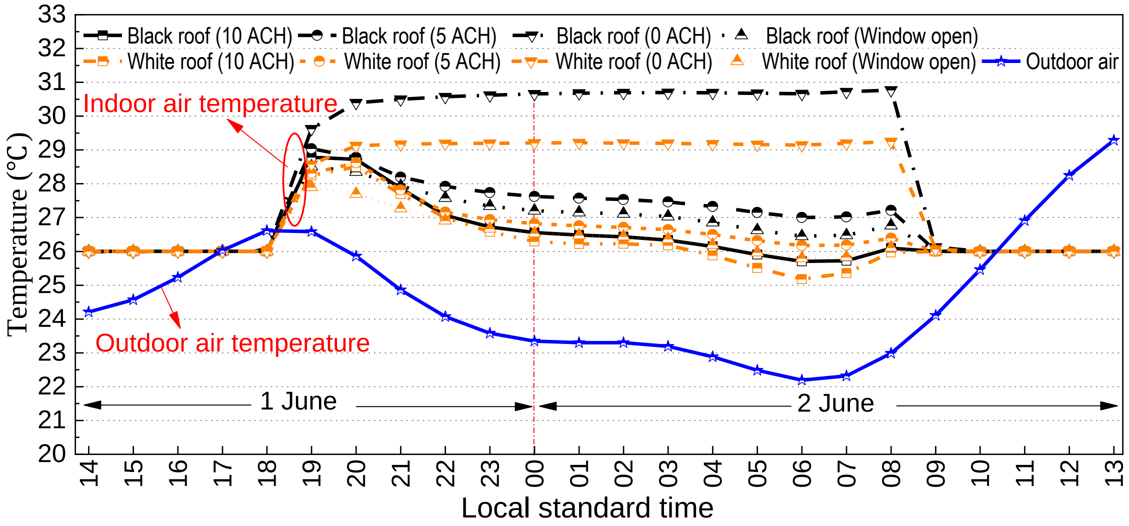

Fig. 11. Indoor air temperature comparison of adopting different strategies in a typical summer night (1 June to 2 June).

3.3 Impacts of concerned parameters on energy and thermal comfort performance

Fig. 12 shows the influences of the concerned parameters on the building energy and thermal comfort performance by comparing the values of Standardized Regression Coefficient (SRC)

(R^2=0.95). It can be seen that the roof albedo has the most significant impact on the annual cooling energy use, followed by the night ventilation ACH, roof insulation level and internal thermal mass level. The roof albedo also has the most significant impact on the POR, followed by the roof insulation level and internal thermal mass level. The SRC values of roof albedo indicate that increasing the roof albedo can significantly decrease the annual cooling energy use but increase the POR. This is due to the high-reflective roof which can reduce solar heat gains and the indoor air temperature, thus reducing the energy consumption in hot days and increasing the indoor uncomfortable time in cold days. It is worth noticing that although the increasing roof albedo can improve the indoor thermal comfort in some days in a transition season, it would also lower the indoor thermal comfort level in non-AC operation periods. In addition, due to the solar heat gain through the roof is high for top-floor rooms, the roof albedo can affect the indoor environment of top-floor rooms significantly. Compared with roof albedo, night ventilation ACH has smaller impacts on the annual cooling energy use and near no influence on the POR. The reason is that the night ventilation cooling potentials are restricted to the days that have cooling demand, while the night ambient temperature in those days is relatively high in Xiamen.

The increase of roof insulation results in more cooling energy use, but to improve the indoor thermal environment during occupied hours in cold days. Although the high roof insulation level can reduce the indoor heat gain at daytime, it prevents the indoor heat dissipation at night. Therefore, the indoor air temperature at next daytime would be higher, which consumes more cooling energy in hot days but reduces the uncomfortable time in cold days. Furthermore, the internal thermal mass has only a slight influence on building energy and thermal comfort performance. Improving the internal thermal mass level is not a preferable choice for buildings under the climate conditions in Xiamen. One possible reason is that the high-level thermal mass stores excess heat gains that cannot be fully removed by night cooling, resulting in more cooling energy use in the following day. Another reason is that the high thermal mass would reduce the fluctuation of indoor air temperature by absorbing and storing the heat energy, resulting in a lower temperature during occupied hours in cold days.

Xiamen’s weather is dominated by a monsoonal humid subtropical climate [57], with an annual mean relative humidity of 70.5% [37]. The high indoor air relative humidity in Xiamen may influence the thermal property of thermal mass, thus affecting the process of charging and discharging heat of thermal mass in practical applications. In this study, a common heat balance algorithm namely “Conduction Transfer Function (CTF)”, which only considers the sensible heat and ignores the moisture storage or diffusion, was selected rather than the “Combined Heat and Moisture Finite Element (CHMFE)” heat balance algorithm [33]. The first reason is that further material properties related to the moisture transfer or diffusion are required when adopting the CHMFE algorithm, which are difficult to obtain without material testing. The second reason is that most research related to the night ventilation mainly focus on the charging and discharging of the sensible heat in the thermal mass, such as the common night ventilation control strategy shown in Table 7. The third reason is that the simulation adopting the CHMFE algorithm may increase the computational cost than the CTF algorithm would. In addition, building energy simulations were conducted to investigate the influence of the indoor air relative humidity on the internal thermal mass energy performance. Two cases were analysed: one case adopted CHMFE algorithm and the other case did not adopt CHMFE algorithm. The internal thermal mass was equipped with the required material properties of one concrete retrieved from an original example in EnergyPlus. The results show that the increase of internal thermal mass level would consume more cooling energy in both two cases. However, the energy increased ratios (defined as the increased annual cooling energy use of using the heavy thermal mass to that using the light thermal mass) are very close in two cases. Therefore, as the SRCs of the internal thermal mass for the energy and thermal comfort performance were both only 0.1, the influence of the indoor air relative humidity was not taken into consideration.

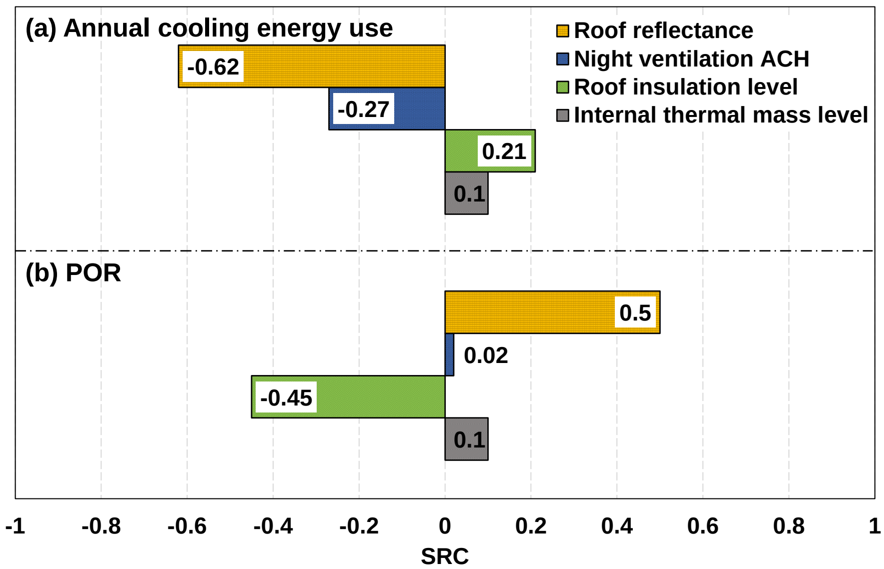

Fig. 12. Standardized Regression Coefficients (SRC) of concerned parameters.

3.4 Design optimization results

The multi-objective optimization approach was also applied to optimize the concerned parameters that would influence the energy and thermal-comfort performance of the buildings. Fig. 13 shows the best Pareto-front sets obtained are shown in. The two objectives – annual cooling energy use and POR during occupied hours without AC operation are inversely proportional, representing the conflicts between the pair of objectives. Two optimal solutions, which achieve minimum annual cooling energy use and POR respectively, are chosen as representative design alternatives for designers. The two solutions are marked as A and B in Fig. 13 and listed in Table 12.

Solution A offers superior energy performance and worst indoor thermal comfort among all the solutions, while Solution B offers superior indoor thermal comfort and worst indoor energy performance among all optimal solutions. In Solution A, the roof albedo is the high bound value (0.9), while the insulation level and internal thermal mass level are the low bound values. In contrast, in Solution B, the roof albedo is the low bound value (0.1), while the insulation level and internal thermal mass level are high bound values. It is worth noting that night ventilation ACH in Solution A is 9.5 h^{-1} that is close to the high bound value of 10 h^{-1}, while the night ventilation ACH in Solution B is 7 h^{-1}. The night ventilation ACH is required to be set at relatively high values among all solutions.

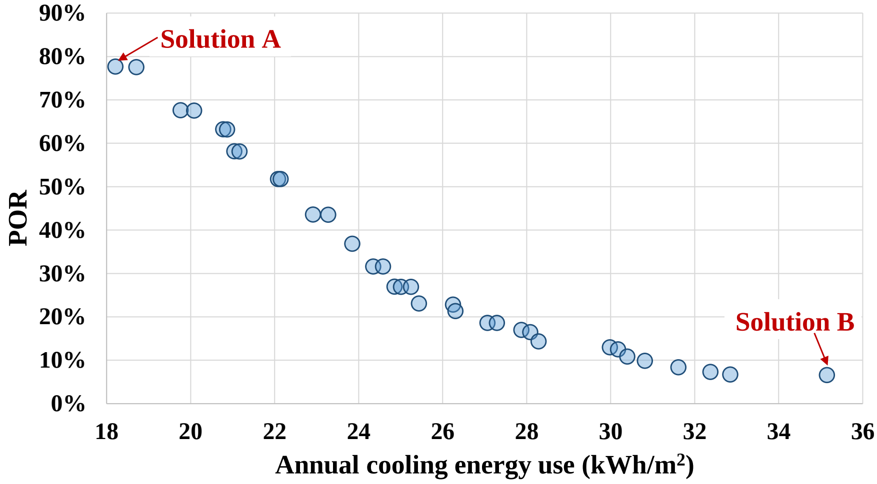

Fig. 13. The optimal solutions on the Pareto front.

Table 12 Selected optimal solutions of the design optimization.

Solution	Roof albedo	Night ventilation ACH	Roof insulation level (mm)	Internal thermal mass level (m^2)	Annual cooling energy use (kWh/m^2)	POR (%)

A	0.9	9.5	10	10	18.2	77.7
B	0.1	7	50	80	35.2	6.6

Fig. 14 shows the objective values under different weights (w_1) of normalized annual cooling energy use (Eq. 7) using the TOPSIS decision-making method. The weight of normalized POR (w_2) equals to (1-w_1). The building designers or owners can select the optimal solutions based on their own requirements and which objective they concern more. In this study, the w_1 of 0.5 is selected to obtain the optimal design parameters and corresponding objective values as shown in Table 13. For the purpose of comparison, the parameters of the base case were set as roof albedo of 0.1, night ventilation ACH of 0 h^{-1}, roof insulation level (represented by the thickness of the insulation board) of 30 mm and internal thermal mass level (represented by the surface area of the cast concrete) of 50 m^2. It can be seen that the values of the two objectives are both lower than that of the base case (i.e. reduction of 10.9 kWh/m^2 (28%) annual cooling energy use and 0.2% uncomfortable time). The solution indicates that the night ventilation ACH, roof insulation level should be as high as possible, while the internal thermal mass level should be as low as possible. The roof albedo of 0.6 can make a compromise between the energy and thermal comfort performance of buildings.

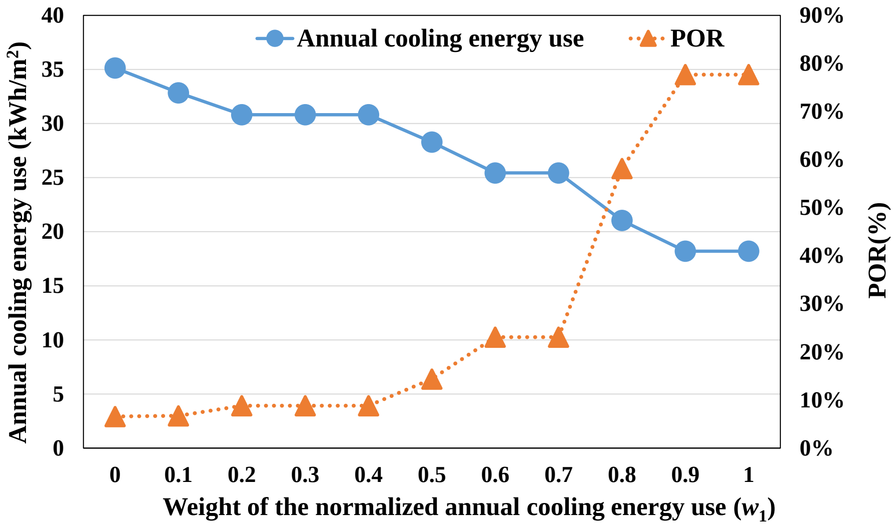

Fig. 14. The objective values under different weights (w_1) of normalized annual cooling energy use.

Table 13 Optimum design parameters and corresponding objective values (w_1=*0.5*).

Design parameter	Unit	Base case	Optimum design
Roof albedo	-	0.1	0.6

Night ventilation ACH	h^{-1}	0	10
Roof insulation level	mm	30	50
Internal thermal mass level	m^2	50	10
Objective	Unit	Base case	Optimum design
Annual cooling energy use	kWh/m^2	39.2	28.3
POR	%	14.5	14.3

4 Conclusions

This study proposes a systematic approach to quantitively evaluate and optimize the cooling potential through the combined use of cool roofs and night ventilation. A six-story office building located in Xiamen, located in a cooling-dominated region, is selected for both experimental and simulation studies. An energy simulation based on the validated model from the experimental data was conducted to investigate the annual energy-saving potential of adopting the cool roof with night cooling. Then, a global sensitivity analysis was carried out to explore the effects of roof albedo, roof insulation, building thermal mass and night ventilation air change rate on the energy and thermal performance of the building. The key design parameters are then optimized. Based on the results of the case study, the following conclusions can be made.

- The experimental study shows that applying cool roofs can significantly reduce the top and bottom surface temperatures of roofs, the indoor air temperatures in the unconditioned rooms and the cooling energy use in the conditioned rooms. In a transient season, the tops of the white roof and yellow roof can be up to 27.2 °C and 20.3 °C cooler, respectively, than the top of the black roof. The bottom (room-facing surfaces) of the white roof and yellow roof can be up to 3.1°C and 2.8°C cooler, respectively, than the bottom of the black roof. The integration of the natural ventilation and cool roof can dissipate unwanted internal heat significantly. In the hot summer from 11 August to 21 August 2015, the white and yellow roof can reduce room cooling energy consumption by 30% and 25% (99 $Wh/m^2\cdot day$ and 82 $Wh/m^2\cdot day$) respectively compared with the black roof.
- The annual energy simulation results show that the combined use of the cool roof and night natural ventilation can achieve the energy-saving rate 27% compared to using a black roof and 13% compared to using a cool roof. Night mechanical ventilation is not energy conservative because the energy consumed by the fan exceeds the cooling energy saved.

- The global sensitivity analysis indicates that the roof albedo is the most influential parameter for building energy performance and indoor thermal comfort. The night ventilation air change rate has also significant impacts on the annual cooling energy use but nearly no influence on the POR. Although more cooling energy use is required, the indoor thermal comfort can be improved through increasing roof insulation level. Improving the internal thermal mass level is not a preferable choice for buildings under climate conditions such as Xiamen.
- The optimum alternative using TOPSIS decision-making method shows that the night ventilation ACH and roof insulation level should be as high as possible, while the roof internal thermal mass level should be as low as possible. The roof albedo should be properly set by compromising the indoor thermal comfort and annual cooling energy use. Additionally, the results of multi-objective optimization obtained by TOPSIS decision-making method shows that the annual cooling energy use decreases greatly 10.9 kWh/m^2 (28%) and the POR brings down slightly 0.2% respect to the base design case.

In this study, thermal/energy performance evaluation and design optimization of these two technologies are conducted in the climate conditions of Xiamen. For cities with similar climatic conditions, the applications of the coupled technologies are expected to have similar energy-saving potentials. However, the expected energy-saving potentials of combined use of cool roof and night ventilation are limited to actual climatic conditions. For other climatic conditions, the performance and optimal design alternatives of utilizing these two technologies can be further explored using the quantitative methods proposed in this study. For instance, for a climate where the heating system is available for buildings in cold seasons, the increased heating energy use caused by high roof albedo may outweigh the cooling energy saving caused by high roof albedo. The cool roof technology may not be suitable for the application in buildings. The annual HVAC (heating, ventilation and air conditioning) source energy use/cost would be the only objective to be optimized since the HVAC system would regulate the indoor thermal comfort. For a climate with hot summer days and cool summer nights, where night ventilation might be more useful than that in Xiamen, the night mechanical ventilation may save energy. The thermal/energy performance of the combined use of these two technologies under different climate conditions are required to be investigated.

Acknowledgments

This research work was supported by the National Natural Science Foundation of China (No. 51878088) and the Chinese Scholarship Council (CSC No. 201706050001). This research was also supported by the Assistant Secretary for Energy Efficiency and Renewable Energy, Building Technologies Office of the U.S. Department of Energy under Contract No. DE-AC02-05CH11231. Special thanks to Binbin Li, Junzhi Peng, Jianmin Tu and Yaping Wang, from Xiamen Academy of Building Research Group Co. for their support in the initiation of this project.

Appendix A. Technique for Order of Preference by Similarity to Ideal Solution (TOPSIS)

The TOPSIS technique involves the following five steps to choose the best alternative nearest to the positive ideal solution and furthest from the negative ideal solution. The best one of sorting would be the best alternative.

Step 1: A multiple attribute decision can be expressed in a matrix *S* with *m* alternatives and *n* attributes. In this study, *n* is the number of objectives needed to be optimized and *m* is the number of optimal solutions on the Pareto front. An element x_{ij} in the matrix represents the numerical value of *i* th alternative, A_i, with respect to the *j* th attribute, B_j, calculated by Eq. (A-1). The matrix S can be normalized to value r_{ij} by Eq. (A-2).

$$S = \begin{pmatrix} & B_1 & B_2 & \cdots & B_j & \cdots & B_n \\ A_1 & x_{11} & x_{12} & \cdots & x_{1j} & \cdots & x_{1n} \\ A_2 & x_{21} & x_{22} & \dots & x_{2j} & \dots & x_{2n} \\ A_3 & x_{31} & x_{32} & \dots & x_{3j} & \dots & x_{3n} \\ \vdots & \vdots & \vdots & \cdots & \vdots & \cdots & \vdots \\ A_m & x_{m1} & x_{m2} & \cdots & x_{mj} & \cdots & x_{mn} \end{pmatrix} \quad \text{(A-1)}$$

$$r_{ij} = \frac{x_{ij}}{\sqrt{\sum_{i=1}^{m} x_{ij}^2}}, i = 1, \dots, m; j = 1, \dots, n \quad \text{(A-2)}$$

Step 2: The weighted normalized value v_{ij} is calculated by Eq. (A-3), where w_j is the weight value of *j*th attribute and $\sum_{j=1}^{n} w_j = 1$. In this study, w_1 means the weight of normalized annual cooling energy use, while w_2 represents the weight of normalized POR during occupied hours without AC operation.

$$v_{ij=}w_j r_{ij}, i = 1, \dots, m; j = 1, \dots, n \quad \text{(A-3)}$$

Step 3: Determining the positive ideal (A^+) and negative ideal (A^-) solutions by Eq. (A-4) and Eq. (A-5).

$$A^+ = \{v_1^+, v_2^+, \ldots, v_n^+\} \quad \text{(A-4)}$$

$$A^- = \{v_1^-, v_2^-, \ldots, v_n^-\} \quad \text{(A-5)}$$

where:

$$v_j^+ = \left[\max (v_{ij}, i \in I \; or \; \min\left(v_{ij}\right), j \in J\right] \quad \text{(A-6)}$$

$$v_j^- = \left[\max (v_{ij}, i \in I \; or \; \min\left(v_{ij}\right), j \in J\right] \quad \text{(A-7)}$$

where I and J are the benefit attributes and cost attributes, respectively. A larger value of I or smaller value of J indicates better performance. In this study, the two objectives both belong to the benefit attributes.

Step 4: Calculating the separation of each alternative from the positive and negative ideal solution, which can be measured by the n dimensional Euclidean distance as follows:

$$s_i^+ = \sqrt{\sum_{j=1}^{n} (v_{ij} - v_j^+)^2}, i = 1,2, \ldots, m \quad \text{(A-8)}$$

$$s_i^- = \sqrt{\sum_{j=1}^{n} (v_{ij} - v_j^-)^2}, i = 1,2, \ldots, m \quad \text{(A-9)}$$

Step 5: Defining the relative closeness to the ideal solution and ranking the preference order by Eq. (A-10). Where the value of c_i it in the range from 0 to 1. Based on the relative closeness value, then ranking the preference order. The larger the value of c_i, the better the performance of the alternatives as it is closer to the positive ideal solution.

$$c_i = \frac{d_i^-}{d_i^- + d_i^+}, i = 1,2, \ldots, m \quad \text{(A-10)}$$

References

[1] L. Pérez-Lombard, J. Ortiz, C. Pout, A review on buildings energy consumption information, Energy Build. 40 (2008) 394–398. https://doi.org/10.1016/j.enbuild.2007.03.007.

[2] Z. Yang, A. Ghahramani, B. Becerik-Gerber, Building occupancy diversity and HVAC (heating, ventilation, and air conditioning) system energy efficiency, Energy. 109 (2016) 641–649. https://doi.org/10.1016/j.energy.2016.04.099.

[3] D. Thevenard, S. Cornick, Revising ASHRAE climatic data for design and standards - Part 1: Overview and data, ASHRAE Trans. 119 (2013) 181–193. http://web.a.ebscohost.com/ehost/detail/detail?vid=0&sid=71b25922-0b96-4276-88c7-

525f2ef489f3%40sessionmgr4008&bdata=JnNpdGU9ZWhvc3QtbGl2ZQ%3D%3D#AN=96045758&db=aph.
[4] D. Kolokotsa, M. Santamouris, S.C. Zerefos, Green and cool roofs' urban heat island mitigation potential in European climates for office buildings under free floating conditions, Sol. Energy. 95 (2013) 118–130. https://doi.org/10.1016/j.solener.2013.06.001.
[5] Y. Gao, D. Shi, R. Levinson, R. Guo, C. Lin, J. Ge, Thermal performance and energy savings of white and sedum-tray garden roof: A case study in a Chongqing office building, Energy Build. 156 (2017) 343–359. https://doi.org/10.1016/j.enbuild.2017.09.091.
[6] K.T. Zingre, M.P. Wan, S. Tong, H. Li, V.W.C. Chang, S.K. Wong, W.B. Thian Toh, I.Y. Leng Lee, Modeling of cool roof heat transfer in tropical climate, Renew. Energy. 75 (2015) 210–223. https://doi.org/10.1016/j.renene.2014.09.045.
[7] H. Akbari, R. Levinson, Evolution of cool-roof standards in the US, Adv. Build. Energy Res. 2 (2008) 1–32. https://doi.org/10.3763/aber.2008.0201.
[8] H. Akbari, R. Levinson, L. Rainer, Monitoring the energy-use effects of cool roofs on California commercial buildings, Energy Build. 37 (2005) 1007–1016. https://doi.org/10.1016/j.enbuild.2004.11.013.
[9] Y. Gao, J. Xu, S. Yang, X. Tang, Q. Zhou, J. Ge, T. Xu, R. Levinson, Cool roofs in China: Policy review, building simulations, and proof-of-concept experiments, Energy Policy. 74 (2014) 190–214. https://doi.org/10.1016/j.enpol.2014.05.036.
[10] A.L. Pisello, M. Santamouris, F. Cotana, Active cool roof effect: impact of cool roofs on cooling system efficiency, Adv. Build. Energy Res. 7 (2013) 209–221. https://doi.org/10.1080/17512549.2013.865560.
[11] E. Shaviv, A. Yezioro, I.G. Capeluto, Thermal mass and night ventilation as passive cooling design strategy, Renew. Energy. 24 (2001) 445–452. https://doi.org/10.1016/S0960-1481(01)00027-1.
[12] M. Fordham, Natural ventilation, Renew. Energy. 19 (2000) 17–37. https://doi.org/10.1016/S0960-1481(99)00012-9.
[13] R. Barzin, J.J.J. Chen, B.R. Young, M.M. Farid, Application of PCM energy storage in combination with night ventilation for space cooling, Appl. Energy. 158 (2015) 412–421. https://doi.org/10.1016/j.apenergy.2015.08.088.
[14] V. Geros, M. Santamouris, A. Tsangrasoulis, G. Guarracino, Experimental evaluation of night ventilation phenomena, Energy Build. 29 (1999) 141–154. https://doi.org/10.1016/S0378-7788(98)00056-5.
[15] M. Santamouris, A. Sfakianaki, K. Pavlou, On the efficiency of night ventilation techniques applied to residential buildings, Energy Build. 42 (2010) 1309–1313. https://doi.org/10.1016/j.enbuild.2010.02.024.
[16] I. Oropeza-Perez, P.A. Ostergaard, Energy saving potential of utilizing natural ventilation under warm conditions - A case study of Mexico, Appl. Energy. 130 (2014) 20–32. https://doi.org/10.1016/j.apenergy.2014.05.035.
[17] M. Kolokotroni, A. Aronis, Cooling-energy reduction in air-conditioned offices by using night ventilation, Appl. Energy. 63 (1999) 241–253. https://doi.org/10.1016/S0306-2619(99)00031-8.
[18] M.H. Chung, J.C. Park, Development of PCM cool roof system to control urban heat island considering temperate climatic conditions, Energy Build. 116 (2016) 341–348. https://doi.org/10.1016/j.enbuild.2015.12.056.
[19] G. Zhou, Y. Yang, H. Xu, Energy performance of a hybrid space-cooling system in an office building using SSPCM thermal storage and night ventilation, Sol. Energy. 85 (2011) 477–485. https://doi.org/10.1016/j.solener.2010.12.028.

[20] E. Solgi, R. Fayaz, B.M. Kari, Cooling load reduction in office buildings of hot-arid climate, combining phase change materials and night purge ventilation, Renew. Energy. 85 (2016) 725–731. https://doi.org/10.1016/j.renene.2015.07.028.
[21] M. Jaworski, Thermal performance of building element containing phase change material (PCM) integrated with ventilation system - An experimental study, Appl. Therm. Eng. 70 (2014) 665–674. https://doi.org/10.1016/j.applthermaleng.2014.05.093.
[22] Y.B. Seong, J.H. Lim, Energy saving potentials of phase change materials applied to lightweight building envelopes, Energies. 6 (2013) 5219–5230. https://doi.org/10.3390/en6105219.
[23] L. Jiang, M. Tang, Thermal analysis of extensive green roofs combined with night ventilation for space cooling, Energy Build. 156 (2017) 238–249. https://doi.org/10.1016/j.enbuild.2017.09.080.
[24] A. Niachou, K. Papakonstantinou, M. Santamouris, A. Tsangrassoulis, G. Mihalakakou, Analysis of the green roof thermal properties and investigation of its energy performance, Energy Build. 33 (2001) 719–729. https://doi.org/10.1016/S0378-7788(01)00062-7.
[25] M.M. AboulNaga, S.N. Abdrabboh, Improving night ventilation into low-rise buildings in hot-arid climates exploring a combined wall-roof solar chimney, in: Renew. Energy, 2000: pp. 47–54. https://doi.org/10.1016/S0960-1481(99)00014-2.
[26] J. Ran, M. Tang, Passive cooling of the green roofs combined with night-time ventilation and walls insulation in hot and humid regions, Sustain. Cities Soc. 38 (2018) 466–475. https://doi.org/10.1016/j.scs.2018.01.027.
[27] D.B. Crawley, L.K. Lawrie, F.C. Winkelmann, W.F. Buhl, Y.J. Huang, C.O. Pedersen, R.K. Strand, R.J. Liesen, D.E. Fisher, M.J. Witte, J. Glazer, EnergyPlus: Creating a new-generation building energy simulation program, Energy Build. 33 (2001) 319–331. https://doi.org/10.1016/S0378-7788(00)00114-6.
[28] ASTM E903-12, Standard Test Method for Measuring Solar Reflectance of Horizontal and Low-Sloped Surfaces in the Field, American Society for Testing and Materials, West Conshohocken, PA, 2012. https://www.astm.org/Standards/E903.htm.
[29] ASTM G173-03(2012), Standard tables for reference solar spectral irradiances: direct normal and hemispherical on 37° tilted surface, American Society for Testing and Materials West Conshohocken, PA, 2012. http://www.astm.org/cgi-bin/resolver.cgi?G173.
[30] ASTM C1371-15, Standard test method for determination of emittance of materials near room temperature using portable emissometers, American Society for Testing and Materials, West Conshohocken, PA, 2015. http://www.astm.org/cgi-bin/resolver.cgi?C1371.
[31] S.B. Ronnen Levinson, Hashem Akbari, Steve Konopacki, Inclusion of Solar Reflectance and Ther-mal Emittance Prescriptive Requirements for Residential Roofs in Title 24, Berkeley, California, USA, 2002. https://www.osti.gov/servlets/purl/813562.
[32] F. Flourentzou, J. Van der Maas, C.-A. Roulet, Natural ventilation for passive cooling: measurement of discharge coefficients, Energy Build. 27 (1998) 283–292. https://doi.org/10.1016/s0378-7788(97)00043-1.
[33] U. Department of Energy, EnergyPlus, Simulation Program v8.9, (2017). https://energyplus.net/documentation.
[34] D. Coakley, P. Raftery, M. Keane, A review of methods to match building energy simulation models to measured data, Renew. Sustain. Energy Rev. 37 (2014) 123–141. https://doi.org/10.1016/j.rser.2014.05.007.
[35] J.S. Haberl, D.E. Claridge, C. Culp, ASHRAE's Guideline 14-2002 for Measurement

of Energy and Demand Savings: How to Determine What Was Really Saved by the Retrofit, 2005. https://oaktrust.library.tamu.edu/handle/1969.1/5147.
[36] J. Sproul, M.P. Wan, B.H. Mandel, A.H. Rosenfeld, Economic comparison of white, green, and black flat roofs in the United States, Energy Build. 71 (2014) 20–27. https://doi.org/10.1016/j.enbuild.2013.11.058.
[37] World Meteorological Organization, WMO Country Profile Database, (2018). https://cpdb.wmo.int/.
[38] EN 15251, Indoor environmental input parameters for design and assessment of energy performance of buildings addressing indoor air quality, thermal environment, lighting and acoustics, (2007). https://webshop.ds.dk/Default.aspx?ID=219&GroupID=91.040.01&ProductID=M204572.
[39] R. Yao, B. Li, K. Steemers, A. Short, Assessing the natural ventilation cooling potential of office buildings in different climate zones in China, Renew. Energy. 34 (2009) 2697–2705. https://doi.org/10.1016/j.renene.2009.05.015.
[40] Ministry of Housing and Urban-Rural Development of the People's Republic of China, GB 50736-2012: Design code for heating ventilation and air conditioning of civil buildings, (2012). https://www.codeofchina.com/standard/GB50736-2012.html.
[41] International Energy Agency, Technical note AIVC 65 - Recommendations on specific fan power and fan system efficiency, 2009. https://www.aivc.org/sites/default/files/members_area/medias/pdf/Technotes/TN65_Specific Fan Power.pdf.
[42] M.A. J, Control of natural ventilation, 1995. https://www.bsria.co.uk/information-membership/bookshop/publication/control-of-natural-ventilation/.
[43] N. Artmann, H. Manz, P. Heiselberg, Climatic potential for passive cooling of buildings by night-time ventilation in Europe, Appl. Energy. 84 (2007) 187–201. https://doi.org/10.1016/j.apenergy.2006.05.004.
[44] A. O'Donnavan, A. Belleri, F. Flourentzou, G.-Q. Zhang, G.C. da Graca, H. Breesch, M. Justo-Alonso, M. Kolokotroni, M.Z. Pomianowski, P. O'Sullivan, others, Ventilative Cooling Design Guide: Energy in Buildings and Communities Programme. March 2018, Aalborg University, Department of Civil Engineering, 2018. https://venticool.eu/wp-content/uploads/2016/11/VC-Design-Guide-EBC-Annex-62-March-2018.pdf (accessed April 15, 2019).
[45] A.H.C. van Paassen, S.H. Liem, B.P. Gröninger, Control of night cooling with natural ventilation. Sensitivity analysis of control strategies and vent openings, 19 Annu. AIVC Conf. (1998) 28–30. https://www.aivc.org/resource/control-night-cooling-natural-ventilation-sensitivity-analysis-control-strategies-and-vent.
[46] F.J. Martin A, Night-cooling strategies. BSRIA technical appraisal 14/96, BSRIA, 1996.
[47] H. Breesch, A. Janssens, Performance evaluation of passive cooling in office buildings based on uncertainty and sensitivity analysis, Sol. Energy. 84 (2010) 1453–1467. https://doi.org/10.1016/j.solener.2010.05.008.
[48] European Commission - IPSC, E.C.- IPSC, Simlab 2.2: Reference Manual, (2008). https://ec.europa.eu/jrc/en/samo/simlab.
[49] Y. Zhang, JEPlus User's Manual v1.7, JEPlus. (2016). http://www.jeplus.org/wiki/doku.php?id=docs:manual_1_7.
[50] T. Wei, A review of sensitivity analysis methods in building energy analysis, Renew. Sustain. Energy Rev. 20 (2013) 411–419. https://doi.org/10.1016/j.rser.2012.12.014.
[51] D.W. Yarbrough, R.W. Anderson, Use of radiation control coatings to reduce building air-conditioning loads, Energy Sources. 15 (1993) 59–66.

https://doi.org/10.1080/00908319308909011.
[52] S. Carlucci, L. Pagliano, A review of indices for the long-term evaluation of the general thermal comfort conditions in buildings, Energy Build. 53 (2012) 194–205. https://doi.org/10.1016/j.enbuild.2012.06.015.
[53] A. Standard, ASHRAE Standard 55-2010: Thermal Environmental Conditions for Human Occupancy, 2010. https://www.ashrae.org/technical-resources/bookstore/standard-55-thermal-environmental-conditions-for-human-occupancy.
[54] Y. Zhang, Use jEPlus as an efficient building design optimisation tool, in: CIBSE ASHRAE Tech. Symp., 2012: pp. 1–12. http://www.jeplus.org/wiki/lib/exe/fetch.php?media=docs:072v1.pdf.
[55] K. Deb, A. Pratap, S. Agarwal, T. Meyarivan, A fast and elitist multiobjective genetic algorithm: NSGA-II, in: IEEE Trans. Evol. Comput., Institute of Electrial and Elecroics Engineers, 2002: pp. 182–197. https://doi.org/10.1109/4235.996017.
[56] C.-L. Hwang, K. Yoon, Multiple attribute decision making: methods and applications a state-of-the-art survey, Springer Science & Business Media, 2012. https://www.springer.com/gp/book/9783540105589.
[57] L. Tang, Y. Zhao, K. Yin, J. Zhao, Xiamen, Cities. 31 (2013) 615–624. https://doi.org/10.1016/j.cities.2012.09.001.

***Declaration of Interest Statement**

Declaration of interests

☒ The authors declare that they have no known competing financial interests or personal relationships that could have appeared to influence the work reported in this paper.